ICESat-2 Precision Orbit Determination

T.C. Thomas[1], S.B. Luthcke[2], T.A. Pennington[3], J.B. Nicholas[1], D.D. Rowlands[2]

[1] Emergent Space Technologies, Inc. @ NASA Goddard Space Flight Center, Greenbelt, Maryland, USA.

[2] Geodesy and Geophysics Laboratory, NASA Goddard Space Flight Center, Greenbelt, Maryland, USA.

[3] KBRWyle @ NASA Goddard Space Flight Center, Greenbelt, Maryland, USA.

Corresponding author: Taylor C. Thomas (taylor.c.thomas@nasa.gov)

Key Points

- ICESat-2 surface return elevation accuracy depends directly on the performance and accuracy of precisely positioning the instrument.
- ICESat-2 mission Precision Orbit Determination (POD) requirement is 3.0 cm radial RMS over a 24-hr. period.
- ICESat-2 POD performance is achieving a factor of 2 improvement over the mission requirement at 1.5 cm radial RMS.

Abstract

The ICESat-2 Precision Orbit Determination (POD) system computes the precise position of the laser altimeter instrument in inertial space, a measurement necessary for accurate geolocation of individual photon surface returns. ICESat-2 POD solutions are generated by the reduction of Global Positioning System (GPS) double-difference carrier phase observable residuals with NASA Goddard Space Flight Center's GEODYN software. Independent satellite laser ranging (SLR) measurements are withheld from the POD solutions and used as an independent arbiter of POD performance. Measurement model updates in the form of estimated GPS antenna phase center and satellite laser ranging retro-reflector tracking point offset vectors as well as a GPS antenna phase center variation map have led to significant improvement in POD performance. GPS residual analysis and orbit precision analysis show no significant anomalous temporal or geographic POD performance issues. The independent SLR residual analysis indicates that POD solutions have achieved a radial orbit accuracy just below 1.5 cm, thus exceeding the mission radial orbit accuracy requirement of 3.0 cm by more than a factor of 2. Future POD processing updates have been identified and will lead to even further improvements in POD performance.

1. Introduction

The National Aeronautics and Space Administration (NASA) launched the Ice, Cloud, and land Elevation Satellite-2 (ICESat-2) on September 15, 2018 with the primary goal of measuring ice sheet topographic change (Neumann et al., 2019). The fundamental measurement used to achieve mission science objectives is the round-trip time of flight of a photon that has been reflected from the Earth's surface after having been transmitted by the Advanced Topographic Laser Altimeter System (ATLAS) (Markus et al., 2017). The location of the point of reflection on the Earth's surface (the bounce point) is determined by the process of geolocation. Geolocation is computed as a function of three measurements: (1) the position of the laser altimeter instrument in inertial space, (2) the pointing of each of the six individual laser beams in inertial space, and (3) the photon event round trip travel time observation measured by the ATLAS instrument (Luthcke et al., 2019a). ICESat-2 Precision Orbit Determination (POD) is responsible for computing the first of these; the precise position of the laser altimeter instrument.

In order to meet the laser surface return elevation accuracies required by the mission science, ICESat-2 has a stringent radial orbit accuracy requirement of 3.0 cm RMS over a 24-hr orbit solution. ICESat-2 POD solutions are computed using the near-continuous Global Positioning System (GPS) tracking data collected by one of the two redundant dual-frequency GPS receiver-antenna systems. Satellite laser ranging (SLR) to the observatory nine corner cube Laser Retro-Reflector (LRR) is withheld from the POD solutions and used as independent validation of orbit performance. After on-orbit measurement modeling improvements, orbit precision and tracking data residual analysis indicate ICESat-2 is exceeding the mission requirement by over a factor of two. Future POD processing updates will lead to still further improvement in orbit accuracy.

2. Tracking Data

2.1. Spacecraft Body-Fixed Coordinate System and Hardware

POD processing utilizes a spacecraft body-fixed coordinate system known as the Observatory Coordinate System (OBS). The OBS +Z-axis points nominally in the nadir direction. The spacecraft body-fixed axis that points nominally in the velocity direction depends on the sun-orbit geometry or the angle between the sun vector and the orbit plane (β' angle). The β' angle varies slowly with a period of ~502 days. Positive β' implies that the OBS +X-axis points nominally in the velocity direction ("flying forwards"), while negative β' implies that the OBS -X-axis points nominally in the velocity direction ("flying backwards"). Around the time when the β' angle crosses 0°, the spacecraft is commanded to perform a yaw-flip maneuver, a 180° rotation about the OBS Z-axis.

ICESat-2 flies in a near-circular (eccentricity = 0.001398), near-polar (inclination angle = 92°), low-Earth orbit (semi-major axis = 6855.9539 km, altitude = ~496 km). Other orbital parameters include longitude of the ascending node = 0°, argument of periapsis = 90°, and mean anomaly = 180°. It is also a frozen orbit with a repeat cycle of 91 days.

The ICESat-2 solar array is oriented in two distinct modes based on β' angle. Airplane mode occurs when the absolute value of the β' angle is less than ~33°. In airplane mode, the solar array is oriented nominally in the cross-track direction and rotates continuously such that the side of the solar array containing the fuel cells remains pointed towards the Sun. Sailboat mode occurs when the absolute value of the β' angle is greater than ~33°. In sailboat mode, the solar array is moved 90° such that it is nominally oriented in the along-track direction and it swivels back and forth to keep the side of the solar array containing the fuel cells pointed towards the Sun.

The origin of the OBS system is located at the center of a spherically mounted retro-reflector mirror attached to the spacecraft bus (Saltzman, 2018), as shown in Figure 1. ICESat-2 carries on-board two SODERN HYDRA star trackers and a Northrup Grumman Scalable Space Inertial Reference Unit, whose data is used on-board to compute quaternions that relate the spacecraft body-fixed coordinate system to the J2000 inertial reference system. These quaternions are downlinked to the ground and used in POD processing. The two solar array drive angles (azimuth and elevation) are also downlinked to the ground and used to determine the orientation of the solar array relative to the spacecraft body, critical for accurate force model computations.

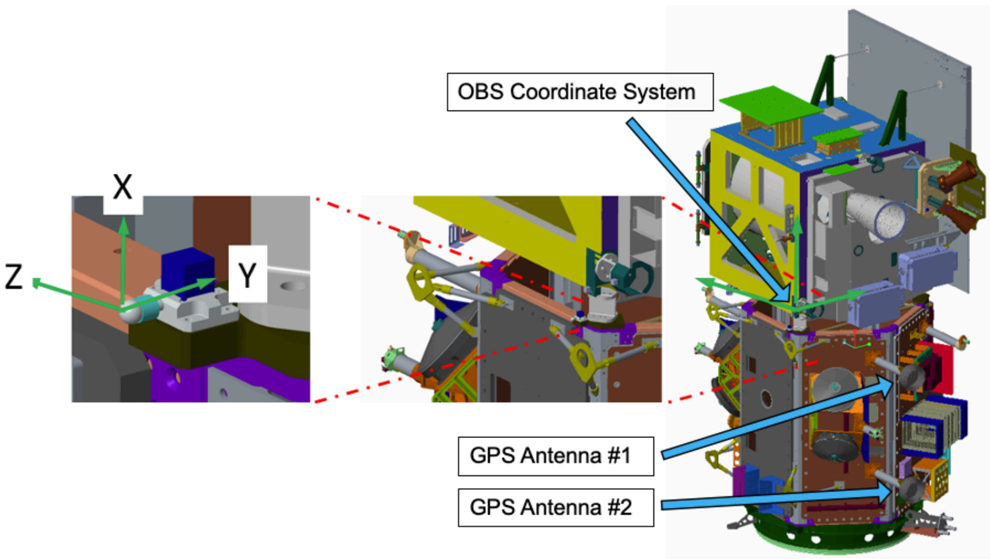

Figure 1 ICESat-2 Observatory Coordinate System and GPS antenna locations.

ICESat-2 also carries on-board two identical geodetic-quality dual-frequency GPS receivers, both manufactured by RUAG Space (Montenbruck et al., 2018). The primary GPS receiver (GPSR1) has been operational throughout the mission, and data from GPSR1 has been used for the computation of all POD solutions to-date. The secondary GPS receiver (GPSR2) was powered on a handful of times during commissioning for dual-GPSR testing (see next paragraph). Each GPS receiver is connected to its own GPS antenna. The locations of the GPS antennas used by GPSR1 and GPSR2 are also identified in Figure 1. Both antennas point in the OBS frame -Z-axis direction (towards zenith), thereby allowing them to track the GPS satellites overhead. ICESat-2 also carries a 9-corner cube SLR LRR manufactured by ITE, Inc. It is located on the OBS +Z-axis side of the spacecraft bus, thereby making it visible to SLR ground tracking stations.

In a standard zero-baseline GPS receiver performance test, two GPS receivers connected to the same antenna collect data simultaneously (deBakker et al., 2009). Double-difference 1-way (DD1W) pseudorange or carrier range observables formed using data from both receivers should show no residual structure as all potential error sources cancel out, thereby allowing for an estimate of the observable noise to be made. The one significant difference between this and the ICESat-2 dual-GPSR tests is that the two ICESat-2 GPS receivers were connected to different GPS antennas separated ~1 meter in the along-track direction. In processing of the L1 C/A carrier phase observables from the dual-GPSR tests, we were able to solve for a relative antenna offset between the two GPS antennas that matched the *a priori* pre-launch measurement of this offset to within 4 mm total magnitude. Carrier phase observable noise estimates from the dual-GPSR tests, 1.9 mm for the L1 frequency and 3.5 mm for the L2 frequency, were also well below the mission's GPS receiver requirements.

2.2. POD Observables

Table 1 presents the details of the POD solutions, including the fundamental observables acquired by the GPS receiver and those used in the POD solutions. The primary measurements reduced in the POD solutions are DD1W GPS carrier phase observables with the ionosphere-free linear combination applied. The double-difference eliminates the direct effect of clock errors in GPS range (phase) observations. Clock errors in the both the GPS satellites and receivers cause an error in the range observation that is the speed of light times the error in time. Clock errors also cause a second order effect. Time tags errors in the receivers cause the measurement model to be degraded. In the pre-processing stage the time tags of the receivers are corrected using *a priori* knowledge of the GPS satellite orbits together with pseudoranges. The ionosphere-free linear combination eliminates, to first order, measurement errors due to carrier phase advance in the ionosphere. A schematic showing the four range measurements involved in forming a DD1W observable is provided in Figure 2. Single-differenced 1-way GPS carrier phase observables (SD1W) have also been used for testing purposes, which eliminates the need for GPS ground station data.

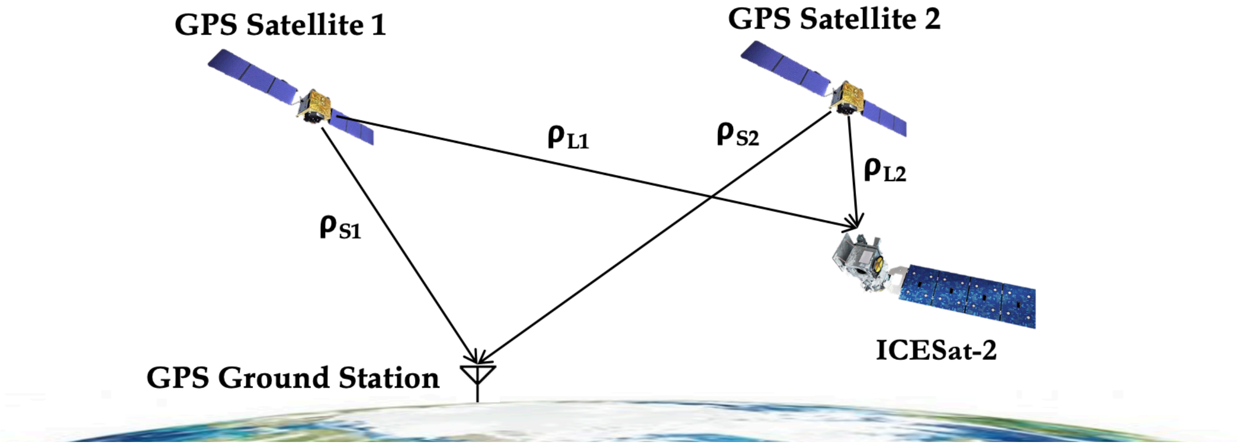

Figure 2 GPS double-difference 1-way range (DD1W) observable schematic. Range (ρ) observable subscript convention: S = Station, L = LEO satellite (ICESat-2), 1 or 2 = GPS satellite number.

All GPS receivers involved, both those on-board ICESat-2 and those at the ground stations, experience cycle slips in carrier phase observables over individual passes. ICESat-2 POD processing involves multiple iterations of orbit solutions; in one of the earlier iterations cycle slips are identified from discontinuities in residuals. These are then resolved by breaking data passes at the cycle slip location and constraining changes in carrier phase ambiguity biases within the pass to allow for an admissible jump in cycles.

SLR ranging measurements are withheld from the POD solutions and used for independent orbit validation. A schematic showing the SLR 2-way range observable is given in Figure 3.

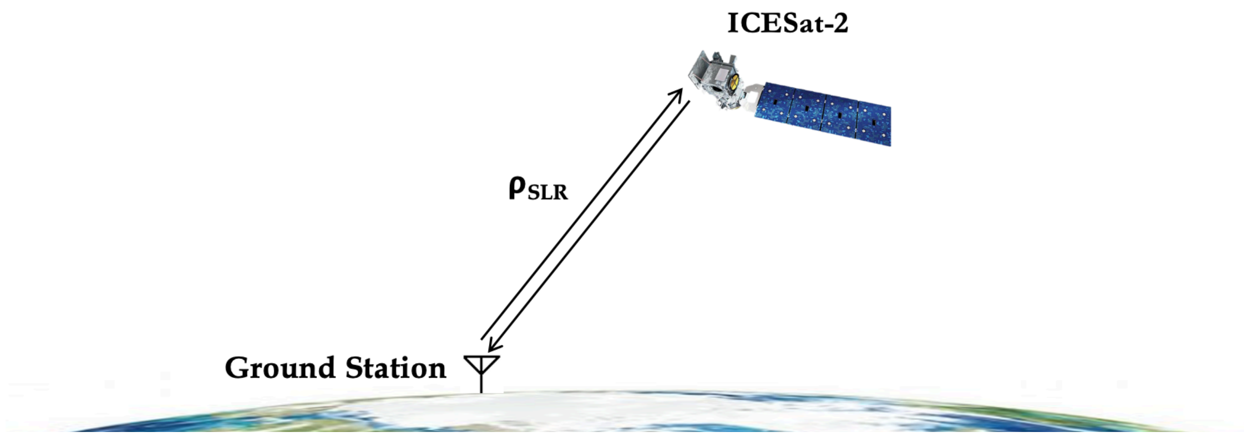

Figure 3 SLR 2-way range observable schematic.

2.3. GPS and SLR Ground Stations

GPS data from 40 ground tracking stations that are part of the International GNSS Service's (IGS) global network are used in the POD processing. The 40 stations were selected based on station performance (quantity and quality of available data), while also maximizing geographic coverage. The names, locations, and tracking residual performance of the 40 selected stations are shown in Figure 4.

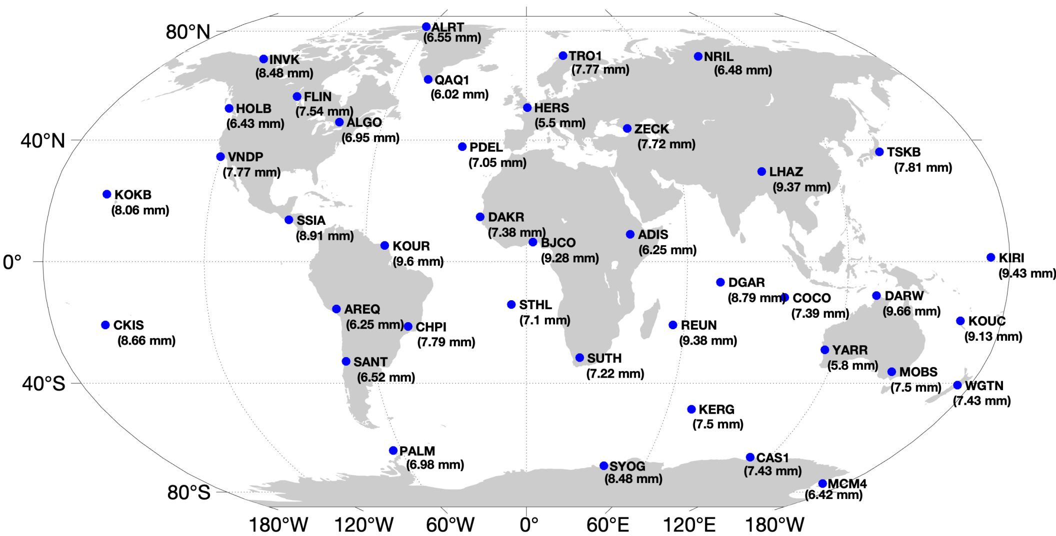

Figure 4 GPS ground station locations and tracking residual performance.

There are currently 11 SLR ground stations that are approved to track ICESat-2. The names and locations of these stations, as well as their tracking residual performance, are shown in Figure 5. In order to avoid damaging the ATLAS instrument detectors with laser energy from ground tracking stations, all SLR stations are restricted to track ICESat-2 up to a maximum local elevation angle of 65°. The exception to this requirement is the SOSW station (7837) located in

Wettzell, Germany. SOSW uses a laser with a wavelength of 849.8 nm, far from the ICESat-2 laser wavelength of 532 nm and thereby efficiently filtered by the instrument optics.

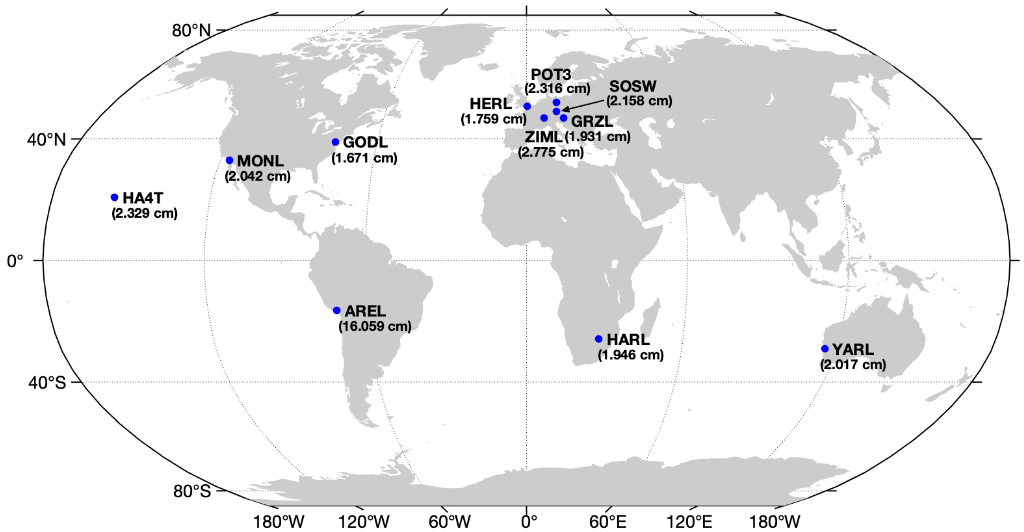

Figure 5 SLR ground station locations and tracking residual performance.

3. Methodology

3.1. Nominal Processing Strategy

POD solutions are generated using GEODYN, NASA Goddard Space Flight Center's (GSFC) orbit determination and geodetic parameter estimation software. GEODYN utilizes a Bayesian least-squares batch estimation process to minimize the GPS DD1W range residuals (Luthcke et al. 2003). A reduced-dynamic solution strategy is employed, where 1-cycle per revolution (1-cpr) along-track and cross-track empirical accelerations are estimated approximately every quarter of an orbit revolution applying a nearest neighbor covariance constraint (Rowlands et al., 1997, Luthcke et al., 2003). The geometrically strong and near-continuous GPS tracking data makes reduced dynamic solutions possible (Yunck et al., 1994, Montenbruck et al., 2005). At this time, a single floating point bias is estimated for each pass to account for the integer ambiguities present in each GPS carrier phase measurement used to form the DD1W observation.

The nominal POD is estimated in 30-hour solutions (ARCs) centered at noon of each day. An ARC is defined as the time interval over which the POD solution is made. The ARC start/stop times are modified where required, such as when there are spacecraft maneuvers or significant gaps in the GPS data. POD utilizes IGS data products that are delivered by GPS week, including final GPS satellite orbit products and weekly station SINEX products (see section 3.2 and Table

1). This lends itself well to processing POD solutions in batches by GPS week, with seven 30-hour ARCs during a nominal week.

3.2. Constants, Models, and Standards

A fully detailed description of the POD process can be found in the ICESat-2 POD Algorithm Theoretical Basis Document (Luthcke, et al., 2019b). However, a brief summary of the most relevant and important constants, models, and standards used in the POD processing is provided here in Table 1.

Table 1 ICESat-2 POD constants, models, and observables overview.

GPS Tracking Data Observables and Modeling	
Pre-processed	RINEX-III format: C1C, C1P, C2P, L1C, L1W
Modeled Observable	Primary: Double Difference Lc ionosphere-free (DD1W); 30-s sampling Secondary: Single Difference Lc ionosphere-free (SD1W); 1-s to 30-s sampling
GPS orbits and clocks	IGS final orbit combination: igs*wwwwd*.sp3, igs*wwwwd*.clk
GPS satellite antenna	IGS Phase Center Offset (PCO) and Phase Variation (PV); igs14_*wwww*.atx
GPS satellite attitude	GPS satellite yaw attitude model for nominal periods. (Bar-Sever, 1996) Yaw-attitude model for eclipse periods, applied based upon nominal yaw rates. (Kouba, 2009)
RHC phase rotation correction	Satellite antenna phase wind-up (Wu et al., 1993).
GPS ground station network	ITRF2014 positions and velocities from IGS weekly SINEX files. igs*YY*P*wwww*.ssc.
Station Antenna Reference Point (ARP) eccentricities	IGS SINEX file (igs_une.snx); dN, dE, dU eccentricities applied.
Atmospheric path delay (troposphere)	IERS2010 (Chen and Herring, 1997) gradient mapping function. VMF1 hydrostatic and wet mapping function (Boehm et al., 2006a, and 2006b).
Gravitational delay	Gravitational delay due to Earth modeled. IERS2010.
Satellite Laser Ranging Observables and Modeling	
SLR ranging observations	ILRS normal point data.
Station positions and velocities	ITRF2014; SLRF 2014
Station eccentricities	ILRS. ecc_une.snx/ecc_xyz.snx
Atmospheric propagation delay (troposphere)	Zenith delay model (Mendes and Pavlis, 2004). Mapping function for line-of-sight elevation dependant correction (Mendes et al., 2002).
ICESat-2 Observatory Modeling	
GPS antenna	PCO and PV from pre-launch measurements, and estimated on orbit.
SLR retro-reflector optical center offset vector	Pre-launch measurement, and estimated on orbit.
ICESat-2 attitude	Telemetered spacecraft body-fixed reference frame to inertial reference frame quaternions Telemetered solar array drive angles (for non-conservative force modeling)
Non-conservative force model	Box Wing model based on pre-launch geometry and observatory surface optical properties (Marshall and Luthcke, 1994, and Luthcke et al., 1997). MSIS atmospheric density (Hedin, 1987). Earth re-radiation (Knocke et al., 1988).
Reduced dynamic – empirical accelerations	Along-track and cross-track 1 cycle per revolution general accelerations estimated approximately every 0.25 of an orbit revolution with nearest neighbor covariance constraint (Luthcke et al. 2003).

Center-of-mass	Estimated spacecraft mass and center-of-mass location provided by the Mission Operations Center following each spacecraft maneuver.
General Modeling and Algorithms	
Earth gravity model	EIGEN6C; GM = 398600.4415 km^3/sec^2 ; $C_{2,0}^{tide\text{-}free}$ (eigen-6c) = -4.84165299806
Time-variable gravity model	Contribution from atmosphere, non-tidal oceans, hydrology, and ice. Developed from GRACE analysis and models (Luthcke et al. 2006, Loomis et al. 2019).
Solid Earth and pole tides	IERS2010
Ocean tides	GOT4.8 for short-period (<1.2 cycles per day). Self-consistent equilibrium for: Node, Sa, Ssa. TPX08 for Mm, Mf, Mt.
Planetary ephemerides; N-Body	JPL DE421 (Standish et al., 1998).
Conventional inertial system	J2000 geocentric; mean equator and equinox of 2000 Jan 1.5 (J2000.0). IERS2010.
Precession-nutation	IAU 2000A precession-nutation model (Coppola et al., 2009).
Earth orientation parameters and UT1-TAI	IERS 08 C04. IERS2010 conventions for diurnal, semidiurnal, and long period tidal effects on polar motion and UT1.
Relativistic corrections	IERS2010. Schwarzschild term (acceleration due to point moss of Earth) – secular drift in argument of perigee. Lense-Thirring and de Sitter terms (geodetic precession) – precession of the orbit plane.
Numerical integration	Cowell predictor-corrector; fixed and variable step; equations of motion and variational equations.
Estimation method	Partitioned Bayesian least squares.

One aspect of the modeling that will be discussed further is the ICESat-2 spacecraft macro-model or otherwise known as a box-wing model (Marshall and Luthcke, 1994). Non-conservative forces acting on the ICESat-2 spacecraft (drag, solar radiation pressure, and Earth re-radiation) are modeled using a series of panels that represent the spacecraft bus, the observatory, and the solar array (Luthcke et al., 1997). Each panel has an area and set of surface optical properties. The initial values for these were derived from pre-launch analyses and are provided in Table 2. These values are currently used and held fixed in all POD solutions.

Table 2 ICESat-2 spacecraft macro-model.

Panel	Surface Normal	Area (m^2)	Specular Reflectivity	Diffuse Reflectivity	Emissivity
Observatory, +X	(1,0,0)	3.414	0	1	0.83
Observatory, +Y	(0,1,0)	4.173	0	1	0.83
Observatory, -Y	(0,-1,0)	4.173	0.5	0.5	0.78
Observatory, +Z	(0,0,1)	2.479	0.4	0.6	0.60
Observatory, -Z	(0,0,-1)	2.479	0	1	0.83
S/C Bus, -X	(-1,0,0)	1.369	0	1	0.83
S/C Bus, +Y	(0,1,0)	1.157	0	1	0.83
S/C Bus, +Y/+Z	(0,0.5,0.87)	1.157	0	1	0.83
S/C Bus, -Y/+Z	(0,-0.5,0.87)	1.157	0	1	0.83

S/C Bus, -Y	(0,-1,0)	1.157	0	1	0.83
S/C Bus, -Y/-Z	(0,-0.5,-0.87)	1.157	0	1	0.83
S/C Bus, +Y/-Z	(0,0.5,-0.87)	1.157	0	1	0.83
Solar Array (cells)	Sun	19.214	0.080	0.020	0.780
Solar Array (back)	Anti-Sun	19.214	0.014	0.056	0.750

3.3. Measurement modeling improvements

Data from GPS weeks 2019-2075 (September 16, 2018 – October 19, 2019) were used to estimate the GPS antenna phase center (APC) and SLR LRR tracking point offset vectors, as well as a GPS antenna phase center variation (PCV) map (Luthcke et al., 2003, and Haines et al., 2004). It should be noted that GPS weeks 2019-2075 do not cover a complete β' cycle; very limited data from the sailboat mode regime during positive β' angle was reduced for these solutions. Therefore, a significant number of GPS weeks and POD solutions are independent of the data used in estimating the tracking point offsets and GPS antenna PCV map.

A priori GPS APC and SLR LRR tracking point offset vectors in the OBS coordinate system were available from pre-launch analysis of observatory models. Table 3 shows the *a priori* and estimated (updated) tracking point offset vectors. We know from experience with previous missions that the errors in the a priori estimates requires the estimation of the GPS APC tracking point offset vector once on-orbit, and this estimation should utilize the best orbit solutions and many weeks worth of data over the various observatory attitude modes. For the same reasons, the SLR LRR tracking point offset vector must be estimated to account for the errors in the a priori vector. The GPS APC and SLR LRR are estimated in the same step such that they are consistent with each other. As a reminder, SLR data is down-weighted such that it does not contribute to the orbit solution. Because of this, some of the improvement in SLR residual statistics shown later in this paper will be due to the update of the SLR LRR tracking point offset vector. This essentially removes the mean bias from the SLR residuals used in the estimation (all SLR data from GPS weeks 2019-2075). Once the updated SLR LRR tracking point offset vector was estimated, it was held fixed in all subsequent solutions.

The largest uncertainty with the a priori tracking point offset vector estimates is in the OBS frame x-direction (along-track), which is congruent with the tracking point offset vector updates shown in Table 3. Estimating only the GPS tracking point offset, while leaving the SLR tracking point offset at the a priori, degrades the SLR residuals as both need to be estimated to establish the proper frame relative to the center-of-mass. The co-estimate of the tracking point offset vectors and GPS antenna PCV map consistently improves the POD metrics for data within the parameter solutions and data independent of the parameter solution, as will be demonstrated in the following section. We note that the demonstrated improvement in the SLR residuals is due to the co-estimation of the GPS and SLR tracking point offset vectors and the GPS antenna PCV map.

Table 3 Tracking point offset vector estimation.

	GPSR1 Antenna Phase Center			SLR Retro-Reflector Optical Center		
	X	Y	Z	X	Y	Z
A priori	-24.31 cm	+54.63 cm	-95.52 cm	-128.90 cm	+54.41 cm	+133.60 cm
Updated	-21.33 cm	+54.84 cm	-93.43 cm	-125.14 cm	+52.90 cm	+131.27 cm
Delta	+2.98 cm	+0.21 cm	+2.09 cm	+3.76 cm	-1.51 cm	-2.33 cm

The GPS antenna PCV map was estimated using 1° elevation and azimuth grid size. Linear constraints between neighboring azimuth/elevation points were applied, and a constraint matrix weighting factor was tuned to achieve the final GPS PCV map solution. The PCV map solution was fully iterated, where the PCV map from one iteration was used as the *a priori* for the next full set of POD solutions and then used to estimate the delta PCV map for the next iteration. Three iterations were performed until convergence was reached. Contrary to the estimation of the GPS APC and SLR LRR tracking point offset vectors, the GPS PCV map was estimated from zero *a priori*. Figure 6 shows the final estimated GPS antenna PCV map. Since the GPS antenna is fixed on the spacecraft bus, the spacecraft velocity direction relative to the GPS antenna PCV map changes depending on whether ICESat-2 is flying forwards or backwards.

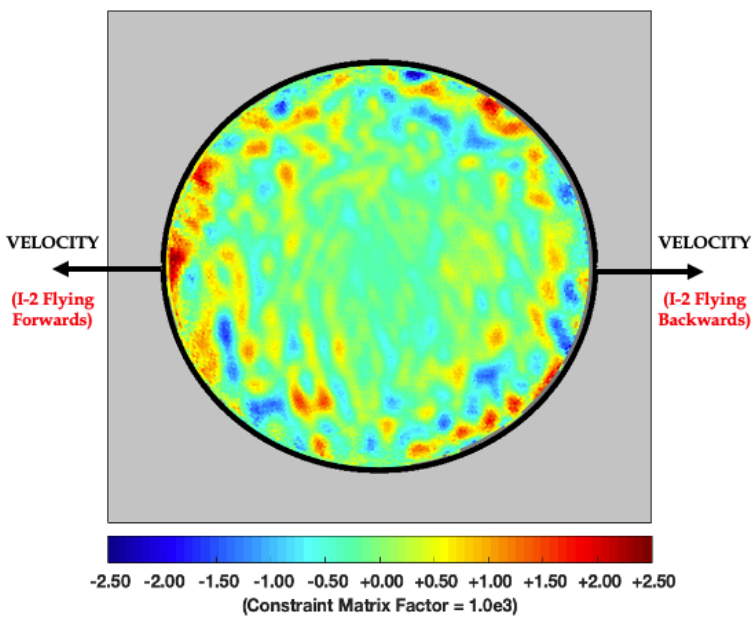

Figure 6 Estimated ICESat-2 GPS antenna PCV map (cm).

4. ICESat-2 POD Performance

ICESat-2 POD performance was assessed over GPS weeks 2019-2105 (September 16, 2018 – May 16, 2020). Two different sets of POD solutions were generated, the results of which are compared throughout the remainder of this article:

- **A priori** = *a priori* GPS & SLR tracking point offset vectors + no GPS PCV map
- **Updated** = updated GPS & SLR tracking point offset vectors + estimated GPS PCV map

4.1. GPS DD1W Range Residuals

Figure 7 shows the average GPS DD1W range residual RMS values per GPS week. The mean over all GPS weeks improves from 0.95 cm to 0.76 cm with the updated GPS/SLR tracking point offset vectors and GPS antenna PCV map included. It is expected that performance would be better during sailboat mode than airplane mode, because the solar array rotates continuously during airplane mode, complicating the non-conservative force modeling. Figure 7 demonstrates a noticeable improvement in the GPS DD1W range residuals during sailboat mode when β' is negative. As mentioned earlier, the GPS/SLR tracking point offset vectors and the GPS antenna PCV map solutions used data from GPS weeks 2019-2075 only. It is likely that this biases the results against the sailboat mode periods when β' is positive. Future POD solutions will utilize GPS antenna estimates from a complete β' cycle, which will improve the consistency of the GPS DD1W RMS values over all sailboat mode periods, both positive and negative β', as compared to airplane mode periods. Consistent improvement in the GPS residuals is seen in GPS weeks 2076-105, which are independent of the GPS antenna tracking point offset vector and GPS antenna PCV map estimations that used data from GPS weeks 2019-2105, certainly providing a strong indication of improved solution performance.

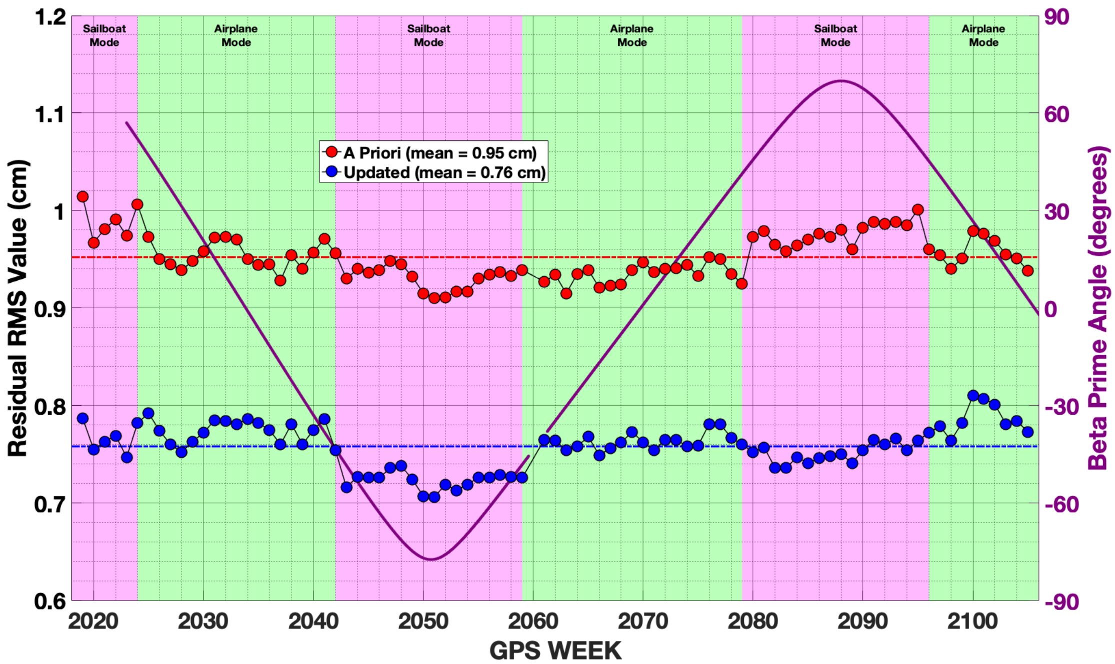

Figure 7 Average GPS DD1W range residual RMS values per GPS week.

Figure 4 shows the GPS ground station locations and their respective GPS DD1W range residual RMS values from the latest set of POD solutions with the updated GPS/SLR tracking point offset vectors and GPS antenna PCV map included. No noticeable discrepancy in GPS DD1W range residual RMS based on geographical location is observed.

4.2. Orbit Precision

The nominal POD strategy utilizes 30-hour ARCs centered at noon of each day. This results in a 6-hour orbit overlap between consecutive ARCs. Because the very tail end of an ARC is usually degraded, the orbit delta during the middle 4-hours of the 6-hour overlap period is used to gauge orbit precision. Figure 8 shows the average consecutive orbit overlap delta per GPS week, both the total 3D positional delta and the radial component only. Results are shown from both the *a priori* and updated POD solutions. There is noticeable improvement in orbit precision with the updated POD solutions that include the updated GPS/SLR tracking point offsets and the GPS antenna PCV map, and the improvement is consistent for both data used in the estimation solutions (GPS weeks 2019-2075) and data independent of the estimation solutions (GPS weeks 2076-2105). The average radial orbit precision in the updated POD solutions is 2.5 mm.

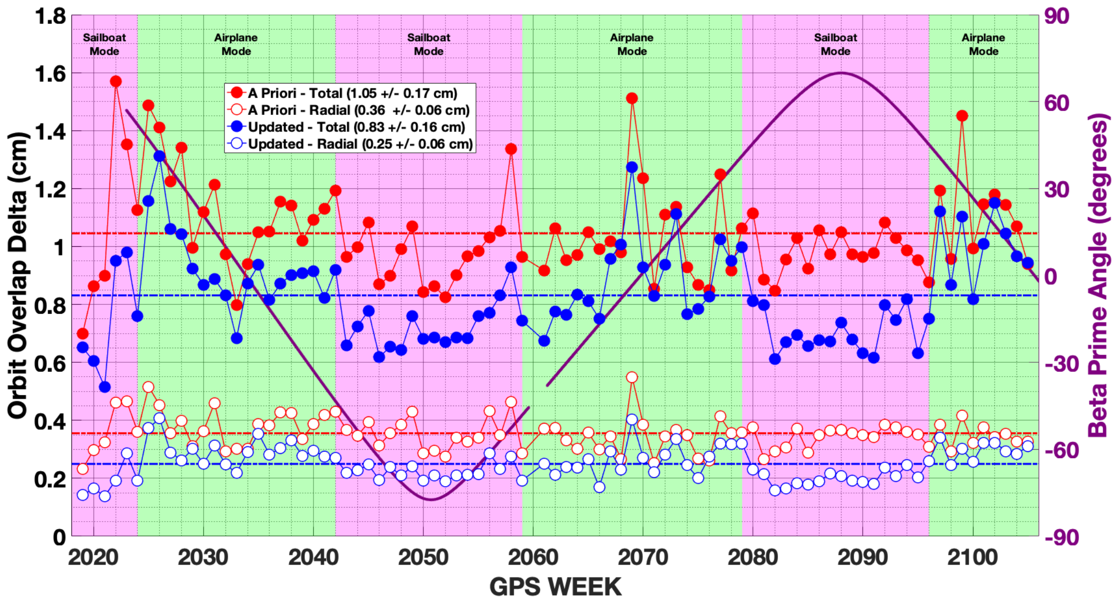

Figure 8 Average consecutive orbit overlap delta per GPS week.

The orbit deltas from all consecutive orbit overlap comparisons were binned by geographical region using 10° latitude/longitude bins. The orbit delta RMS was then computed for each bin. Figure 9 shows the results from both the *a priori* and updated POD solutions. The updated POD solutions improve radial orbit precision consistently across the globe, and there is no strong geographical correlation observed.

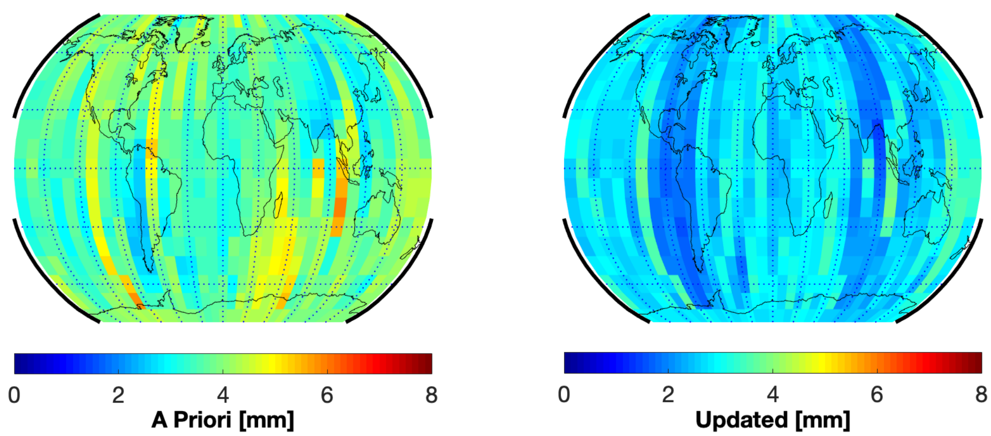

Figure 9 Consecutive orbit overlap delta (radial component) - geographical distribution.

4.3. SLR 2-way Range Residuals

The SLR 2-way range data has not been allowed to contribute to the orbit solution. Instead, the SLR 2-way range data has been used to represent a direct and highly accurate independent arbiter of POD performance. Here we summarize the SLR 2-way range residual performance and the resultant ICESat-2 POD performance. Figure 10 shows the average SLR 2-way range residual RMS per GPS week. The mean over all GPS weeks improves from 2.58 cm to 1.98 cm with the updated GPS/SLR tracking point vectors and GPS antenna PCV map included in the POD solutions. These results are on the same order as seen with other geodetic satellite missions, including the Sentinel missions which also utilize RUAG dual-frequency GPS receivers (Montenbruck et. al, 2018).

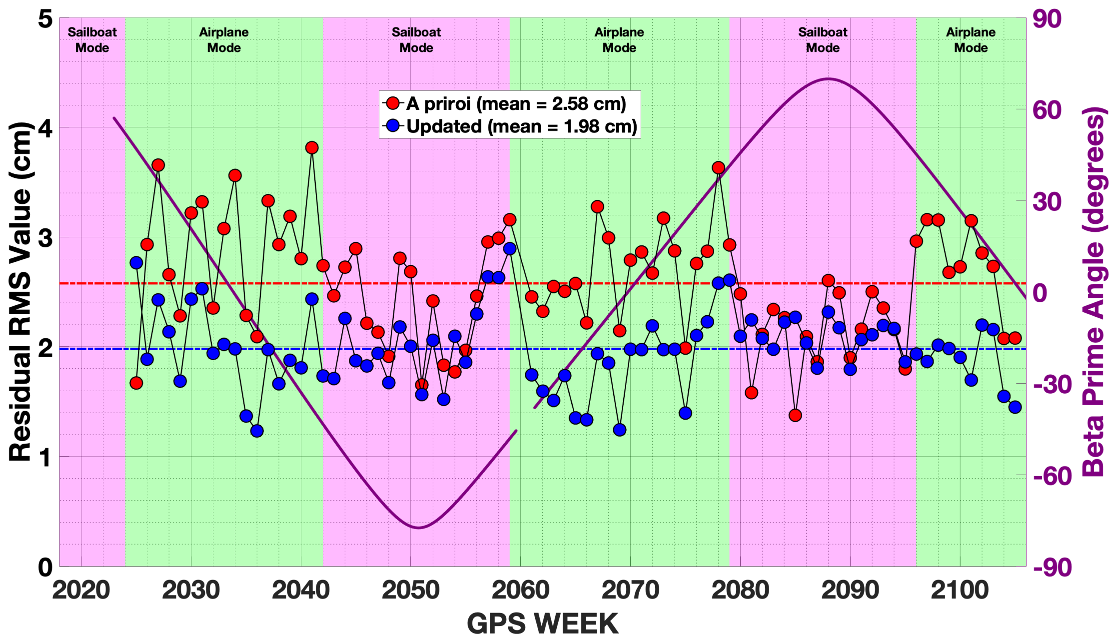

Figure 10 Average independent SLR 2-way range residual RMS values per GPS week.

Table 4 below breaks down the independent SLR residual statistics from the updated set of POD solutions per ground station.

Table 4 Independent SLR residual statistics per ground station.
(*Total does not include results from Arequipa station).

Station Name	Site Code	Station #	Number of Data Points	Residual Mean (mm)	Residual RMS (mm)
Arequipa	AREL	7403	319	55.8	160.6
Graz	GRZL	7839	3,917	4.7	19.3
Greenbelt	GODL	7105	5,402	-6.2	16.7
Haleakala	HA4T	7119	1,639	7.2	23.3
Hartebeesthoek	HARL	7501	2,164	-0.6	19.5
Herstmonceux	HERL	7840	1,114	-7.5	17.6
Monument Peak	MONL	7110	4,211	5.7	20.4
Postdam	POT3	7841	1,416	-15.2	23.2
Wettzell	SOSW	7827	1,074	3.5	21.6
Yarragadee	YARL	7090	24,820	-1.2	20.2

Zimmerwald	ZIML	7810	20	-3.2	27.8
Total*			45,777	-0.8	19.9

Figure 11 shows the independent SLR residuals versus elevation angle from the updated set of POD solutions with the updated GPS/SLR tracking point offset vectors and the GPS antenna PCV map included. Data from all SLR ground tracking stations, with the exception of Arequipa, is included in the figure. Different colors represent data from different stations. As mentioned earlier, the SOSW station is the only one allowed to track above 65° elevation angle, and in Figure 11 there is data of only one color (light green), representing SOSW, that exceeds 65° elevation angle.

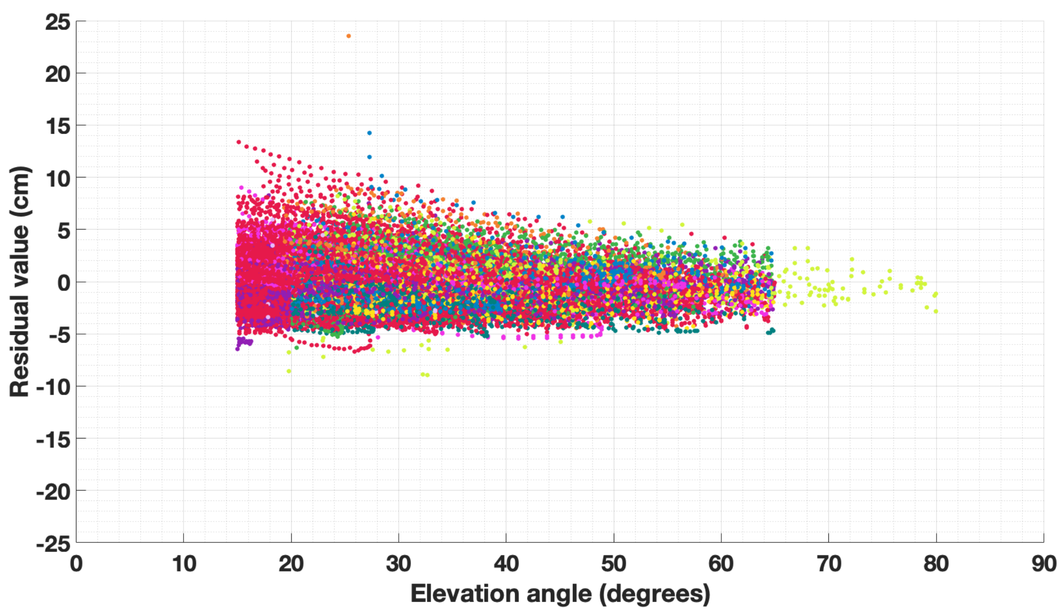

Figure 11 Independent SLR 2-way range residuals versus elevation angle (data from all stations excluding Arequipa).

The independent SLR residuals were sorted into 5° elevation bins, and the residual RMS value was computed per bin. Lower elevation angle implies that the SLR signal passes through the troposphere with a greater range and measures more of the larger along- and cross-track orbit error components than the radial component (Luthcke et al., 2003). It is therefore expected, and confirmed by the results below, that SLR residual RMS values should decrease as local elevation angle at the station increases and measures more directly the radial component of orbit accuracy. As seen Figure 12 below, the SLR residual RMS statistics decrease linearly ($R^2 = 0.866$ in the updated solutions) with increasing elevation angle over elevation angles ranging from 15-65°. While it is not necessarily true that this linear trend continues beyond 65° elevation angle, projecting the SLR residual RMS value to 90° for the updated set of POD solutions (blue) would give a value just below 1.5 cm. At 90° elevation angle only the radial component of the orbit error contributes to SLR measurement errors, leading to the conclusion that ICESat-2 radial orbit accuracy is estimated to be just below 1.5 cm. This is not a perfect test as SLR measurements contain error sources other than radial orbit error, including station position and SLR tracking point offset vector errors (Luthcke et al., 2003). A 1.5 cm radial orbit accuracy is an improvement over the mission requirement of 3.0 cm by a factor of 2.

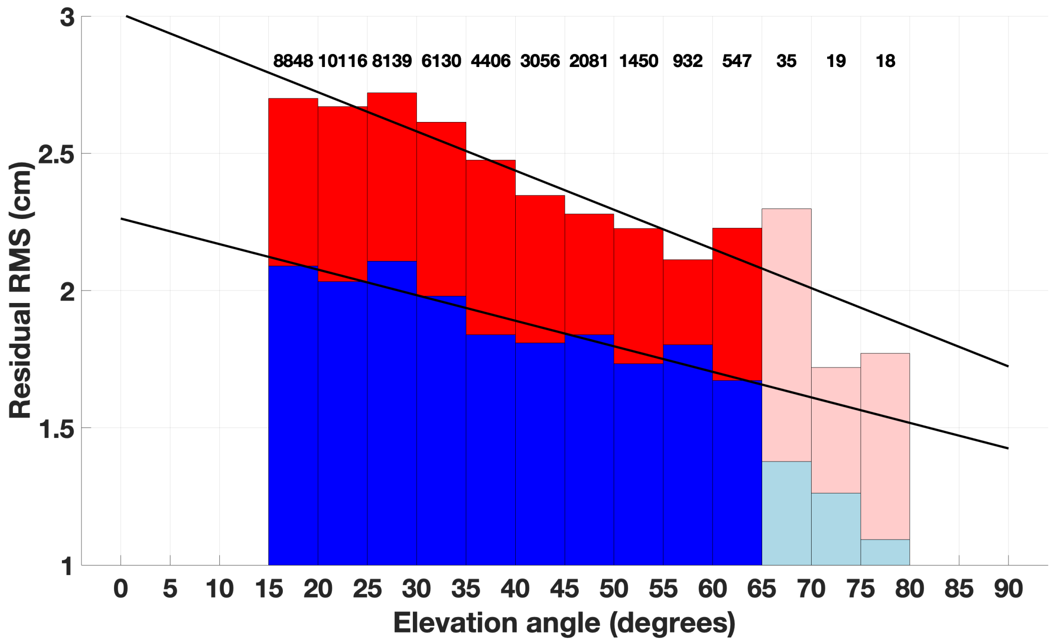

Figure 12 Independent SLR 2-way range residuals versus elevation angle - 5° elevation angle bins (data from all stations excluding Arequipa). Red = *a priori* POD solutions, blue = updated POD solutions. Darker shaded bars used in computing projection to 90° elevation angle.

5. Future Improvements

While the POD solutions have been assessed to be performing better than the mission requirements, there are several planned updates which will further improve POD performance. First, the estimation of the GPS/SLR tracking point offsets and the GPS antenna PCV map were performed using data from only a portion of a β' cycle. These will be re-estimated using data from a full (or multiple) β'cycle(s), which should lead to better consistency in the POD performance across all flying regimes, i.e. sailboat vs. airplane mode, positive vs. negative β' angle.

There are two additional tuning procedures that will be performed. First, the ICESat-2 spacecraft macro-model parameters, presented earlier in Section 3.2, will be tuned as part of the tracking data residual reduction. Second, the reduced-dynamic solution parameterization will be further tuned over a longer time span covering more than one complete β' cycle and utilizing the new measurement and non-conservative force modeling improvements. This involves fine tuning the optimal correlation time and weight parameters for the empirical acceleration neighbor covariance constraints (Rowlands et al., 1997, and Luthcke et al., 2003).

Other planned POD processing and performance assessment updates include: (1) monitoring and improving the GPS ground station selection on a GPS week basis, (2) using high-rate (1 Hz) GPS receiver data in single difference solutions, (3) incorporating resolution of carrier phase data integer ambiguities into the POD solutions, and (4) using laser altimeter data in the form of cross-overs as another data set for performance assessment.

6. Conclusions

The quality of the POD solutions is an indication that the ICESat-2 on-board GPS receiver-antenna and SLR LRR systems, as well as the ground processing system, are functioning well. The POD solutions are generated by minimizing the GPS DD1W range residuals, while withholding SLR 2-way range data for independent orbit validation. On-orbit estimates of the GPS APC and SLR LRR tracking point offsets, as well as the GPS antenna PCV map represent important measurement modeling improvements and have resulted in significant POD performance improvement. GPS residual analysis and orbit precision analysis show no significant anomalous temporal and geographic POD performance issues. The independent SLR data indicates the POD solutions have achieved a radial orbit accuracy just below 1.5 cm using the measurement model improvements. The results demonstrate that the mission radial orbit accuracy performance has achieved a factor of 2 improvement over the mission requirement of 3.0 cm RMS. Future POD improvements have been identified and will lead to even further improvements in POD performance.

Acknowledgments

The specific ICESat-2 datasets used for this research are available at the NASA Distributed Active Archive Center (DAAC) at the National Snow and Ice Data Center (NSIDC). Specifically, the following datasets were used: The ATLAS/ICESat-2 L1B Converted Telemetry Data, Version 3, ATL02 data product, Accessed [https://nsidc.org/data/ATL02/versions/3, global data granules for the time period September 2018 through August 2020], Martino et al., 2020, doi.org/10.5067/ATLAS/ATL02.003.

International GNSS Service (IGS) and Satellite Laser Ranging (SLR) data products used for this research are available at the Crustal Dynamics Data Information System (CDDIS) data center (Noll, 2010). The specific products used are the following:

International GNSS Service, GNSS Daily 30-second Data Product, Greenbelt, MD, USA:NASA Crustal Dynamics Data Information System (CDDIS), Accessed [https://cddis.nasa.gov/archive/gnss/data/daily/, YYYY/DDD/YYt/mmmmDDD#.YYd.Z, global data for the time period September 2019 through August 2020] at doi:10.5067/GNSS/gnss_daily_d_001

International GNSS Service, GNSS Final Combined Orbit Solution Product, Greenbelt, MD, USA:NASA Crustal Dynamics Data Information System (CDDIS), Accessed [https://cddis.nasa.gov/archive/gnss/data/products, WWWW/igsWWWWD.sp3.Z, GPS satellite final orbits for the time period September 2019 through August 2020] at doi:10.5067/gnss/gnss_igsorb_001

International GNSS Service, Final Combined Station Positions/Velocities (no covariance matrix) Product, Greenbelt, MD, USA:NASA Crustal Dynamics Data Information System (CDDIS), Accessed [https://cddis.nasa.gov/archive/gnss/data/products, WWWW/igsyyPwwwwd.ssc.Z, for the time period September 2019 through August 2020] at doi:10.5067/GNSS/gnss_igsssc_001

International Laser Ranging Service (ILRS), SLR daily normal point data, Greenbelt, MD, USA:NASA Crustal Dynamics Data Information System (CDDIS), Accessed [https://cddis.nasa.gov/archive/slr/data/npt_crd/, SATNAME/YYYY/icesat2_YYYYMMDD.npt, for the time period September 2019 through August 2020] at doi:10.5067/SLR/slr_data_daily_npt_001

International Laser Ranging Service (ILRS), SLR monthly normal point data, Greenbelt, MD, USA:NASA Crustal Dynamics Data Information System (CDDIS), Accessed [https://cddis.nasa.gov/archive/slr/data/npt_crd/, SATNAME/YYYY/icesat2_YYYYMM.npt, for the time period September 2019 through August 2020] at doi:10.5067/SLR/slr_data_monthly_npt_001.

International Terrestrial Reference Frame (ITRF), International Satellite Laser Ranging (ILRS) Station positions & velocities, Accessed [http://itrf.ensg.ign.fr/ITRF_solutions/2014/ITRF2014_files.php, ITRF2014-ILRS-TRF.SNX.gz, for the time period September 2019 through August 2020], Altamimi et al., 2016, doi:10.1002/2016JB013098

The authors would like to acknowledge Despina Pavlis (UMD) for her many years of dedicated GEODYN maintenance support.

References

Altamimi, Z., P. Rebischung, L. Metivier, and X. Collilieux (2016), ITRF2014: A new release of the International Terrestrial Reference Frame modeling nonlinear station motions, J. Geophys. Res. Solid Earth, 121, doi:10.1002/2016JB013098.

Bar-Sever, Y.E. (1996), A new model for GPS yaw attitude. *J. of Geodesy*, 70, 714-723. doi:10.1007/BF00867149

Boehm J., Werl, B. , Schuh, H. (2006a). Troposphere mapping functions for GPS and very long baseline interferometry from European Centre for Medium-Range Weather Forecasts operational analysis data. *J. Geophys. Res.*, 111, B02406. doi:10.1029/2005JB003629

Boehm J., Niell, A., Tregoning, P., Schuh, H. (2006b) The Global Mapping Function (GMF): A new empirical mapping function based on data from numerical weather model data. *Geophys. Res. Lett.*, 33 L07304. doi:10.129/2005GL025546

Chen, G., Herring, T.A. (1997), Effects of atmospheric azimuthal asymmetry on the analysis of space geodetic data. *J. of Geophys. Res., Solid Earth*, 102(B9), 20489–20502. doi.org/10.1029/97JB01739

Coppola, V. & Seago, J.H. & Vallado, David. (2009). The IAU 2000A and IAU 2006 precession-nutation theories and their implementation. *Advances in the Astronautical Sciences*. 134. 919-938.

de Bakker, P.F., van der Marel, H. & Tiberius, C.C.J.M. (2009), Geometry-free undifferenced, single and double differenced analysis of single frequency GPS, EGNOS and GIOVE-A/B measurements. *GPS Solut* 13, 305–314. doi.org/10.1007/s10291-009-0123-6

Haines, B., Bar-Sever, Y., Bertiger, W., Desai, S., Willis, P. (2004), One-Centimeter Orbit Determination for Jason1: New GPS-Based Strategies, *Marine Geod*, 27. 299-318. 10.1080/01490410490465300.

Hedin, A. (1987), MSIS-86 Thermospheric Model, *J. Geophys. Res*., 92(A5), 4649-4662. doi.org/10.1029/JA092iA05p04649

Knocke, P.C., J.C. Ries, B.D. Tapley (1988), Earth Radiation Pressure Effects on Satellites, Proceedings of the AIAA/AAS Astrodynamics Conference, 577–586, 1988.

C. Noll (2010), The Crustal Dynamics Data Information System: A resource to support scientific analysis using space geodesy, *Advances in Space Research*, 45(12), 1421-1440, DOI: 10.1016/j.asr.2010.01.018.

Kouba, J. (2009), A simplified yaw-attitude model for eclipsing GPS satellites. *GPS Solut.* 13, 1–12. DOI 10.1007/s10291-008-0092-1

Loomis, B.D., Luthcke, S.B. & Sabaka, T.J. (2019), Regularization and error characterization of GRACE mascons. *J Geod* 93, 1381–1398. doi.org/10.1007/s00190-019-01252-y

Luthcke, S.B., Marshall, J.A., Rowton, S.C., Rachlin, K.E. and Cox, C.M. (1997), Enhanced Radiative Force Modeling of The Tracking and Data Relay Satellites, *J of Astronaut Sci*, 45(3), 349-370. doi.org/10.1007/BF03546409

Luthcke, S.B., Zelensky, N., Rowlands, D.D.. (2003). The 1-cm orbit: Jason-1 precision orbit determination using GPS, SLR, DORIS, and altimeter data. *Marine Geod*.. 26. 261-284. doi: 10.1080/714044529

Luthcke, S.B., D.D. Rowlands, F.G. Lemoine, S.M. Klosko, D. Chinn and J.J. McCarthy (2006), Monthly spherical harmonic gravity field solutions determined from GRACE inter-satellite range-rate data alone, *Geophys. Res. Lett.*, 33, doi:10.1029/2005GL024846.

Luthcke, S., Pennington, T., Rebold, T., Thomas, T. (2019a), ICESat-2 Algorithm Theoretical Basis Document for ATL03g ICESat-2 Receive Photon Geolocation Version 6.0, ICESat-2-SIPS-SPEC-0142

Luthcke, S.B., Pennington, T.A., Rebold, T.W., & Thomas, T.C., (2019b), ICESat-2 Algorithm Theoretical Basis Document for Precision Orbit Determination and Geolocation Parameter Calibration Version 2.0, ICESat-2-SIPS-SPEC-0140

Markus, T., Neumann, T., Martino, A., Abdalati, W., Brunt, K., Csatho, B., Farrell, S., Fricker, H., Gardner, A., Harding, D., Jasinski, M., Kwok, R., Magruder, L., Lubin, D., Luthcke, S., Morison, J., Nelson, R., Neuenschwander, A., Palm, S., Popescu, S., Shum, C.K., Schutz, B.E., Smith, B., Yang, Y., Zwally, H.J. (2017), The Ice, Cloud and land Elevation Satellite-2 (ICESat-2): Science Requirements, Concept, and Implementation. *Remote Sensing of the Environment*, 190, 260-273. doi: 10.1016/j.rse.2016.12.029

Martino, A. J., M. R. Bock, C. Gosmeyer, C. Field, T. A. Neumann, D. Hancock, R. L. Jones III, P. W. Dabney, C. E. Webb, and J. Lee. 2020. *ATLAS/ICESat-2 L1B Converted Telemetry Data, Version 3*. [Global data, Sept. 2018 through August 2020]. Boulder, Colorado USA. NASA National Snow and Ice Data Center Distributed Active Archive Center. doi: https://doi.org/10.5067/ATLAS/ATL02.003. Accessed [September 2018 through August 2020].

Marshall, J.A. and Luthcke, S.B. (1994) Nonconservative Force Model Performance for TOPEX/Poseidon Precision Orbit Determination, *J of Spacecraft and Rockets*, 31(1), 229-246.

Mendes, V.B., and Pavlis, E.C. (2004), High-accuracy zenith delay prediction at optical wavelengths. *Geophys. Res. Lett.*, 31. doi.org/10.1029/2004GL020308

Mendes, V. B., G. Prates, E. C. Pavlis, D. E. Pavlis, and R. B. Langley (2002), Improved mapping functions for atmospheric refraction correction in SLR. *Geophys. Res. Lett*., 29(10), 1414, doi:10.1029/2001GL014394

Montenbruck, O., Helleputte, T. van., Kroes, R., Eberhard, G. (2005), Reduced dynamic orbit determination using GPS code and carrier measurements, Aerospace Sci. and Tech., 9(3), 261-271. doi.org/10.1016/j.ast.2005.01.003

Montenbruck, O., Hackel S., & Jaggi A., (2018), Precise orbit determination of the Sentinel-3A altimetry satellite using ambiguity-fixed GPS carrier phase observations, *J Geod*, 92, 711-726. doi.org/10.1007/s00190-017-1090-2

Neumann, T., Martino, A., Markus, T., Bae, S., Bock, M., Brenner, A., Brunt, K., Cavanaugh, J., Fernandes, S., Hancock, D., Harbeck, K., Lee, J., Kurtz, N., Luers, P., Luthcke, S., Magruder, L., Pennington, T., Ramos-Izquierdo, L., Rebold, T., Skoog, J., Thomas, T. (2019), The Ice, Cloud, and Land Elevation Satellite – 2 Mission: A Global Geolocated Photon Product Derived From the Advanced Topographic Laser Altimeter System, Remote Sensing of Environment, 233, doi:10.1016/j.rse.2019.111325

Rowlands, D.D., Luthcke, S.B., Marshall, J.A., Cox, C.M., Williamson, R.G. and Rowton, S.C. (1997), Space Shuttle Precision Orbit Determination in Support of SLA-1 Using TDRSS and GPS Tracking Data, *Journal of Astronautical Sciences*, 45(1), 113-129. doi.org/10.1007/BF03546384

Saltzman, M., (2018), Coordinate Systems Descriptions Report, ICESat-2-SYS-RPT-4972

Standish, E.M. (1998), JPL Planetary and Lunar Ephemerides, DE405/LE405, JPL IOM 312.F-98-048.

Wu, J.T., Wu, S.C., Hajj, G.A., Bertiger, W.I., Lichten, S.M. (1993), Effects of antenna orientation on GPS carrier phase. *Manuscripta Geodaetica,* 18(2), 91–98.

Yunck, Thomas & Bertiger, W. & Wu, S. & Bar-Sever, Y. & Christensen, E. & Haines, B. & Lichten, Stephen & Muellerschoen, Ronald & Vigue, Y. & Willis, Pascal, (1994). First assessment of GPS-based reduced dynamic orbit determination on TOPEX/Poseidon, *Geophysical Research Letters*. 21. 10.1029/94GL00010.

Acronyms

APC	Antenna Phase Center
ARP	Antenna Reference Point
ATLAS	Advanced Topographic Laser Altimeter System
DD1W	Double-Difference 1-Way
GEODYN	NASA GSFC POD and Geodetic Parameter Estimation Software
GNSS	Global Navigation Satellite System
GPS	Global Positioning System
GPSR	GPS Receiver
GSFC	Goddard Space Flight Center
IAU	International Astronomical Union
IERS	International Earth Rotation and Reference Systems Service
IGS	International GNSS Service
ILRS	International Laser Ranging Service
ITRF	International Terrestrial Reference Frame
LC	Linear Combination
LRR	Laser Retro-Reflector
NASA	National Aeronautics and Space Administration
OBS	Observatory Coordinate System
PCO	Phase Center Offset
PCV	Phase Center Variation
POD	Precision Orbit Determination
PV	Phase Variation

S/C	Spacecraft
SD1W	Single-Difference 1-Way
RINEX	Receiver Independent Exchange format
SINEX	Solution Independent Exchange format
SLR	Satellite Laser Ranging
VMF	Vienna Mapping Function